GEOPHYSICS, VOL. 64, NO. 6 (NOVEMBER–DECEMBER 1999); P. 1928–1938, 21 FIGS., 1 TABLE.

Amplitude-variation-with-angle behavior of self-similar interfaces

Kees Wapenaar*

ABSTRACT

Amplitude-variation-with-angle (AVA) analysis is generally based on the assumption that the medium parameters behave as step functions of the depth coordinate z, at least in a finite region around the interface. However, outliers observed in well logs often behave quite differently from step functions. In this paper, outliers in the acoustic propagation velocity are parameterized by functions of the form $c(z) = c_1 |z/z_1|^{\alpha}$. The wavelet transform of this function reveals properties similar to those of several outliers in real well logs. Moreover, this function is self-similar, according to $c(\beta z) = \beta^{\alpha} c(z)$, for $\beta > 0$. Analytical expressions are derived for the acoustic normal incidence reflection and transmission coefficients for this type of velocity function. For oblique incidence, no explicit solutions are available. However, by exploiting the self-similarity property of the velocity function, it turns out that the acoustic angle-dependent and frequency-dependent reflection and transmission coefficients are self-similar as well. To be more specific, these coefficients appear to be constant along curves described by $p^{1-\alpha}\omega^{-\alpha} = \text{constant}$, where p is the raypath parameter and ω the angular frequency. The singularity exponent α that is reflected in these curves may prove to be a useful indicator in seismic characterization.

INTRODUCTION

Amplitude-variation-with-offset (AVO) analysis or (more accurately) amplitude-variation-with-angle (AVA) analysis is generally based on a model consisting of two homogeneous layers, separated by a horizontal interface (see Castagna and Backus, 1993, chapter I), for an extensive list of references. This implies that the medium parameters are assumed to behave as step functions of the depth coordinate z, at least in a finite region around the interface. Obviously a step function is just one specific example of a more general class of functions that describe the local behavior of the medium parameters. From a theoretical point of view, the step function is a logical choice because it permits a relatively straightforward derivation of the angle-dependent reflection and transmission coefficients (Zoeppritz, 1919; Aki and Richards, 1980). However, looking at well logs of, for example, the compressional wave velocity $c(z)$, it appears that the main outliers, responsible for the main reflections, often behave quite differently from step functions (see Figure 1). Hence, it seems reasonable to investigate the effect of velocity functions other than the step function on AVA. In this paper, outliers will be parameterized by singular functions of the form $c(z) = c_1|z/z_1|^{\alpha}$, where α is the singularity exponent, z_1 is a reference depth, and c_1 a reference velocity. For convenience, the singular point has been chosen at $z = 0$. It appears that the singularity properties of this function, analyzed by the wavelet transform (Mallat and Hwang, 1992), correspond nicely to those of several outliers in real well logs, as analyzed by Herrmann (1997). [This correspondence is observed at wavelengths related to the seismic frequency range. At significantly smaller wavelengths, the correspondence breaks down (one reason being the smoothing effect of the logging tool). See Wapenaar (1998) for further discussion.] Note that the parameterized function is self-similar, according to $c(\beta z) = \beta^{\alpha} c(z)$ for $\beta > 0$ (see Figure 2). This property will be exploited in the derivation of the AVA behavior of the acoustic reflection and transmission coefficients. It will turn out that these coefficients are self-similar as well and that the exponent α appears, not surprisingly, in their self-similarity relations.

WAVE EQUATION FOR VERTICAL PROPAGATION

In this section, the wave equation and its elementary solutions for vertical propagation are considered. For the velocity function $c(z) = c_1|z/z_1|^{\alpha}$ and a constant mass density, the

Presented at the 66th Annual International Meeting, Society of Exploration Geophysicists. Manuscript received by the Editor November 14, 1996; revised manuscript received December 15, 1998.
*Delft University of Technology, Centre for Technical Geoscience, Lab of Seismics and Acoustics, Lorentzweg 1, 2628 CJ Delft, Netherlands. E-mail: c.p.a.wapenaar@ctg.tudelft.nl.

wave equation for the acoustic pressure $P(z,\omega)$ in the space-frequency domain is given by

$$\frac{\partial^2 P}{\partial z^2} + \left(\frac{\omega}{c_1}\right)^2 \left|\frac{z}{z_1}\right|^{-2\alpha} P = 0, \quad \text{for} \quad z \neq 0, \qquad (1)$$

where ω is the angular frequency (throughout this paper only positive ω will be considered). Note that the singular point $z=0$ is excluded; the boundary conditions at this point will be treated in the next section. Making the following substitutions

$$P(z,\omega) = \zeta^{\nu} Q(\zeta), \quad \text{with} \quad \zeta = \chi \left|\frac{z}{z_1}\right|^{\frac{1}{2\nu}}, \qquad (2)$$

$$\chi = \frac{2\omega\nu|z_1|}{c_1} \quad \text{and} \quad \nu = \frac{1}{2-2\alpha}, \qquad (3)$$

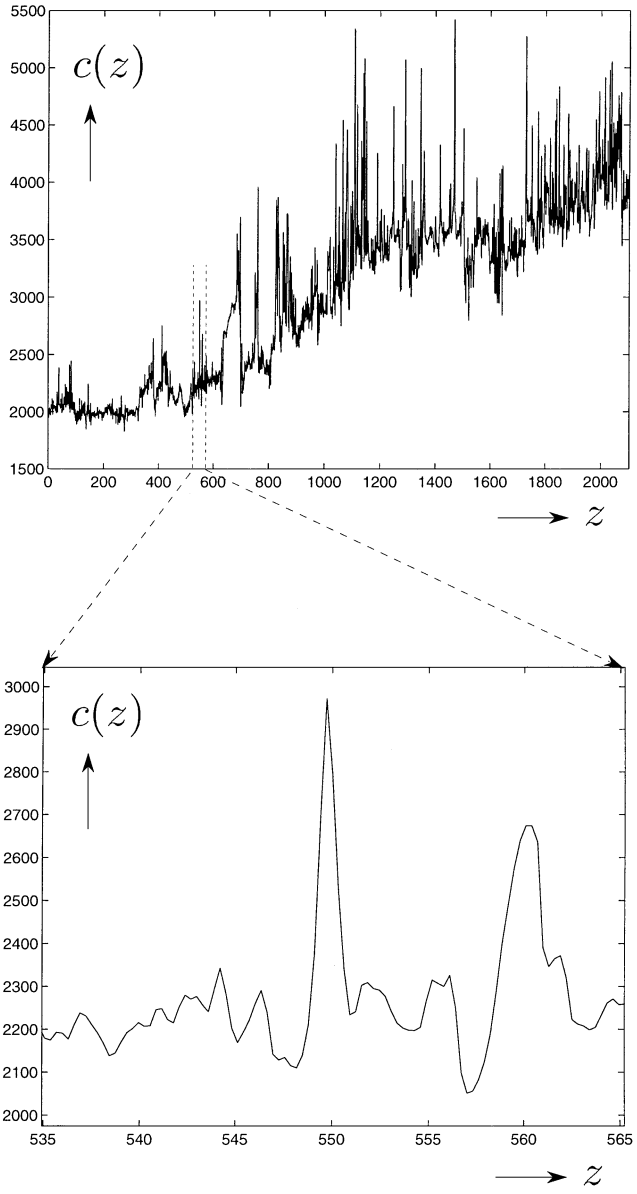

FIG. 1. Well log of P-wave velocity $c(z)$.

yields the Bessel equation for $Q(\zeta)$, according to

$$\zeta^2 \frac{\partial^2 Q}{\partial \zeta^2} + \zeta \frac{\partial Q}{\partial \zeta} + (\zeta^2 - \nu^2) Q = 0, \quad \text{for} \quad \zeta \neq 0, \qquad (4)$$

with real-valued ζ and ν. This equation is satisfied by Bessel functions as well as Hankel functions of order ν (Abramowitz and Stegun, 1970, chapter 9). The general solution of equation (1) can thus be expressed in terms of Hankel functions,

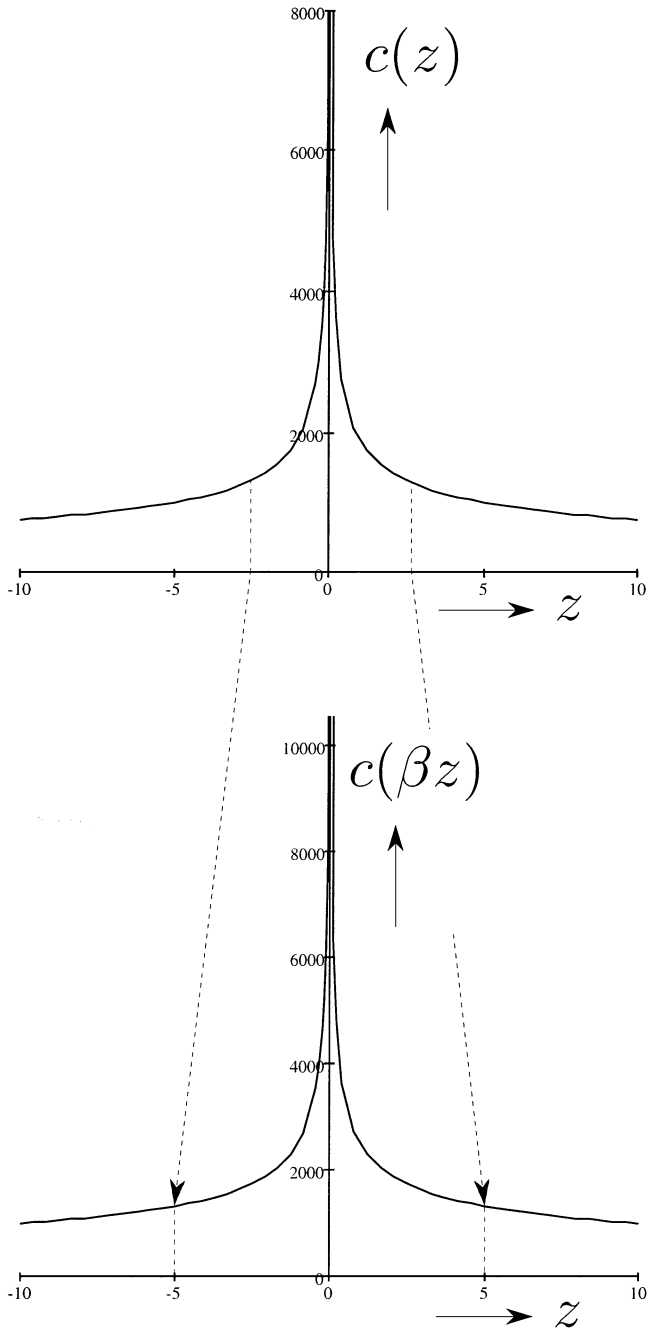

FIG. 2. The self-similar function $c(z) = c_1|z/z_1|^{\alpha}$, with $c_1 = 1000$ m/s, $z_1 = 5$ m, and $\alpha = -0.4$. The "zoom-factor" is chosen as $\beta = 0.5$; hence, the scaling factor β^{α} equals 1.32.

according to

$$P(z,\omega) = g_1(\omega)U(z,\omega) + g_2(\omega)U^*(z,\omega), \quad \text{for} \quad z \neq 0, \tag{5}$$

where

$$U(z,\omega) = \mathrm{e}^{j\psi_\nu}\zeta^\nu \mathrm{H}_\nu^{(1)}(\zeta) \tag{6}$$

and * denotes complex conjugation. In equation (5), $g_1(\omega)$ and $g_2(\omega)$ are arbitrary complex-valued amplitude factors. The phase factor $\mathrm{e}^{j\psi_\nu}$ in equation (6) has been introduced for convenience; a useful choice for ψ_ν will be made later, based on the asymptotic expansion of $U(z,\omega)$.

Note that the elementary solution $U(z,\omega)$ obeys the following similarity relation:

$$U(\beta z,\omega) = U(z,\beta^{1-\alpha}\omega) \tag{7}$$

for $\beta > 0$. When g_1 and g_2 are frequency independent, the same relation applies for $P(z,\omega)$. This will be illustrated with an example in the next section.

For arbitrary self-similar media, Hargreaves (1996) arrived at a similar relation—but with an undetermined power of β—by simple reasoning, starting with the statement that "in a scale-free world, all geophysical observations are scale-free."

The solution presented in equation (6) can be seen as a special case of the Whittaker functions treated by Brekhovskikh and Godin (1990). Those authors use these functions to derive normal incidence reflection coefficients for the situation of a homogeneous upper half-space and a large class of 1-D inhomogeneous lower half-spaces. However, they do not treat configurations in which the velocity is singular, as will be done below. Moreover, in the present paper, the self-similarity property $c(\beta z) = \beta^\alpha c(z)$ will be exploited in the analysis of the AVA behavior of the reflection and transmission coefficients.

This section is concluded by summarizing some properties of the elementary solution $U(z,\omega)$.

Using equation (9.1.27) of Abramowitz and Stegun (1970), the derivative with respect to z is obtained:

$$\frac{\partial U(z,\omega)}{\partial z} = \mathrm{e}^{j\psi_\nu}\zeta^\nu\left(\frac{2\nu}{\zeta}\mathrm{H}_\nu^{(1)}(\zeta) - \mathrm{H}_{\nu+1}^{(1)}(\zeta)\right)\frac{\partial\zeta}{\partial z}, \tag{8}$$

with

$$\frac{\partial\zeta}{\partial z} = \frac{\omega}{c_1}\left(\frac{\zeta}{\chi}\right)^{1-2\nu}\mathrm{sign}(z). \tag{9}$$

With this result and equation (9.1.17) of Abramowitz and Stegun (1970), the power flux $F(z,\omega)$ associated with $U(z,\omega)$ becomes

$$F = \frac{1}{2j\omega\varrho_1}\left(U\frac{\partial U^*}{\partial z} - U^*\frac{\partial U}{\partial z}\right) = \frac{-2\mathrm{sign}(z)}{\pi\varrho_1 c_1}\chi^{2\nu-1}, \tag{10}$$

where ϱ_1 is the (constant) mass density. Note that for negative/positive z, the power flux is positive/negative, which implies that $U(z,\omega)$ may be interpreted as a downgoing/upgoing wave (the z-axis points downward). The opposite applies to $U^*(z,\omega)$.

Using equation (9.2.3) of Abramowitz and Stegun (1970), the following asymptotic expressions for $|z| \to \infty$ and/or $\omega \to \infty$ are obtained:

$$U(z,\omega) \to \sqrt{\frac{2}{\pi}}\zeta^{\nu-\frac{1}{2}}\exp\left[j\left(\zeta + \psi_\nu - \frac{\nu\pi}{2} - \frac{\pi}{4}\right)\right], \tag{11}$$

$$\frac{\partial U(z,\omega)}{\partial z} \to j\frac{\partial\zeta}{\partial z}U(z,\omega). \tag{12}$$

From these expressions, the remarks made above about downgoing and upgoing waves are easily confirmed. From here onward, ψ_ν is chosen to be

$$\psi_\nu = \left(\nu + \frac{1}{2}\right)\frac{\pi}{2}, \tag{13}$$

so that the phase term in equation (11) simplifies to $\exp(j\zeta)$.

Finally, in Appendix A, it is shown that the limits for $|z| \to 0$ read

$$U(z,\omega) \to A = \frac{\mathrm{e}^{j\left(\nu-\frac{1}{2}\right)\frac{\pi}{2}}2^\nu\Gamma(\nu)}{\pi}, \tag{14}$$

$$\frac{\partial U(z,\omega)}{\partial z} \to \frac{2\omega\nu}{c_1}\chi^{2\nu-1}\mathrm{sign}(z)B, \tag{15}$$

$$\text{with} \quad B = \frac{-\mathrm{e}^{-j(\nu+\frac{1}{2})\frac{\pi}{2}}\Gamma(1-\nu)}{2^\nu\nu\pi}, \tag{16}$$

assuming $\alpha < \frac{1}{2}$ (this condition on α will be employed in the remainder of this paper). These limits are essential in the derivation of the normal incidence reflection and transmission coefficients.

NORMAL INCIDENCE REFLECTION AND TRANSMISSION COEFFICIENTS

In this section, it will be assumed that the parameters c_1, ϱ_1, z_1, and α may be different above and below the singular point at $z = 0$. They will be distinguished by a subscript n, with $n = 1$ for the upper half-space $z < 0$ and $n = 2$ for the lower half-space $z > 0$. Hence,

$$c(z) = \begin{cases} c_1|z/z_1|^{\alpha_1} & \text{for } z < 0 \\ c_2|z/z_2|^{\alpha_2} & \text{for } z > 0, \end{cases} \tag{17}$$

with $\alpha_n < \frac{1}{2}$ (the mass density will be parameterized as a step function from ϱ_1 to ϱ_2 throughout this paper). All related variables and functions will be labeled with the corresponding subscript. When only one of the parameters α_1 and α_2 is not equal to zero, the singularity is one-sided; when both are nonzero the singularity is two-sided.

Reflection and transmission coefficients are usually defined in terms of downgoing and upgoing waves at the interface. It is well known that in an inhomogeneous medium, downgoing and upgoing waves are not uniquely defined (Brekhovskikh and Godin, 1990). Based on the observations in the previous section, in this paper the downgoing and upgoing waves will be expressed in terms of $U_n(z,\omega)$ and $U_n^*(z,\omega)$. The reflection and transmission coefficients R^+ and T^+ for an incident downgoing

wave $U_1(z,\omega)$ are introduced via

$$P(z,\omega)=\begin{cases}\mu_1\{U_1(z,\omega)+R^+U_1^*(z,\omega)\}, & \text{for } z<0,\\ \mu_2 T^+U_2^*(z,\omega), & \text{for } z>0,\end{cases} \tag{18}$$

where μ_n is a normalization coefficient, defined as

$$\mu_n=\begin{cases}1/|U_n(0,\omega)|=1/|A_n| & \text{pressure normalization}\\ \sqrt{1/|F_n|}=\sqrt{\dfrac{\pi\varrho_n c_n \chi_n^{1-2\nu_n}}{2}} & \text{power flux normalization.}\end{cases} \tag{19}$$

Since the limits for $|z|\to 0$ of $U_n(z,\omega)$ and its derivative $U_n'(z,\omega)$ exist, it is justified to impose the usual boundary conditions (i.e., to require continuity of the pressure and the vertical component of the particle velocity at the singular point $z=0$). Hence,

$$\mu_1\{U_1(-\epsilon,\omega)+R^+U_1^*(-\epsilon,\omega)\}=\mu_2 T^+U_2^*(\epsilon,\omega), \tag{20}$$

$$\frac{\mu_1}{\varrho_1}\{U_1'(-\epsilon,\omega)+R^+U_1'^*(-\epsilon,\omega)\}=\frac{\mu_2}{\varrho_2}T^+U_2'^*(\epsilon,\omega), \tag{21}$$

for $\epsilon\downarrow 0$. Using equations (14) and (15), this yields

$$1+\frac{A_1^*}{A_1}R^+=\frac{A_2^*}{A_1}\left(\frac{\mu_2}{\mu_1}T^+\right), \tag{22}$$

$$1+\frac{B_1^*}{B_1}R^+=-\frac{B_2^*\nu_2\chi_2^{2\nu_2-1}}{B_1\nu_1\chi_1^{2\nu_1-1}}\frac{\varrho_1 c_1}{\varrho_2 c_2}\left(\frac{\mu_2}{\mu_1}\,T^+\right), \tag{23}$$

or

$$R^+=\frac{-A_2^*B_1\nu_1\chi_2^{1-2\nu_2}\varrho_2c_2-A_1B_2^*\nu_2\chi_1^{1-2\nu_1}\varrho_1c_1}{A_2^*B_1^*\nu_1\chi_2^{1-2\nu_2}\varrho_2c_2+A_1^*B_2^*\nu_2\chi_1^{1-2\nu_1}\varrho_1c_1}, \tag{24}$$

and

$$T^+=\frac{\mu_1}{\mu_2}\left[\frac{(A_1B_1^*-A_1^*B_1)\nu_1\chi_2^{1-2\nu_2}\varrho_2c_2}{A_2^*B_1^*\nu_1\chi_2^{1-2\nu_2}\varrho_2c_2+A_1^*B_2^*\nu_2\chi_1^{1-2\nu_1}\varrho_1c_1}\right]. \tag{25}$$

Note that R^+ and T^+ are related, according to

$$\begin{cases}T^+=e^{j(\nu_1+\nu_2-1)\frac{\pi}{2}}+e^{j(\nu_2-\nu_1)\frac{\pi}{2}}R^+ & \text{pressure normalization}\\ |T^+|=\sqrt{1-|R^+|^2} & \text{power flux normalization.}\end{cases} \tag{26}$$

[The latter result was found from $\mathrm{lhs}_1\mathrm{lhs}_2^*-\mathrm{lhs}_1^*\mathrm{lhs}_2=\mathrm{rhs}_1\mathrm{rhs}_2^*-\mathrm{rhs}_1^*\mathrm{rhs}_2$, where "lhs" and "rhs" stand for lefthand side and righthand side, respectively, and where 1 and 2 refer to equations (20) and (21), respectively.]

In a similar way, reflection and transmission coefficients R^- and T^- for an incident upgoing wave $U_2(z,\omega)$ can be derived.

Two-sided singularity

Note that R^+ and T^+, as given by equations (24) and (25), become frequency independent when the exponents α_1 and α_2 at both sides of the singularity are taken to be equal, i.e., $\alpha_1=\alpha_2=\alpha$ (which implies $\nu_1=\nu_2=\nu$). Choosing $|z_1|=|z_2|$ as well yields

$$R^+=j\left[\frac{e^{-j\nu\pi}\varrho_2c_2^{2\nu}+e^{j\nu\pi}\varrho_1c_1^{2\nu}}{\varrho_2c_2^{2\nu}+\varrho_1c_1^{2\nu}}\right], \tag{27}$$

$$T^+=\begin{cases}\dfrac{2\sin(\nu\pi)\varrho_2c_2^{2\nu}}{\varrho_2c_2^{2\nu}+\varrho_1c_1^{2\nu}} & \text{pressure normalization}\\ \dfrac{2\sin(\nu\pi)\sqrt{\varrho_2c_2^{2\nu}\varrho_1c_1^{2\nu}}}{\varrho_2c_2^{2\nu}+\varrho_1c_1^{2\nu}} & \text{power flux normalization,}\end{cases} \tag{28}$$

$$R^-=-\{R^+\}^*, \tag{29}$$

$$T^-=\begin{cases}\dfrac{\varrho_1c_1^{2\nu}}{\varrho_2c_2^{2\nu}}T^+ & \text{pressure normalization}\\ T^+ & \text{power flux normalization.}\end{cases} \tag{30}$$

For the parameters in Table 1, the modulus and phase of the coefficients R^+ and T^+ are shown in Figure 3 as a function of α.

Note that when both half-spaces are homogeneous (i.e., $\alpha=0\to\nu=\frac{1}{2}$), equations (27) through (30) reduce to the usual expressions for the reflection and transmission coefficients. On the other hand, for $\varrho_1=\varrho_2$, $c_1=c_2$, and arbitrary α, equations (27) through (30) simplify to

$$R^+=R^-=j\cos(\nu\pi), \tag{31}$$

$$T^+=T^-=\sin(\nu\pi), \tag{32}$$

Table 1. Parameter values, used in the examples in this paper.

	$z<0$ $(n=1)$	$z>0$ $(n=2)$
c_n (m/s)	800	1200
ϱ_n (kg/m^3)	1000	1000
z_n (m)	−5	5

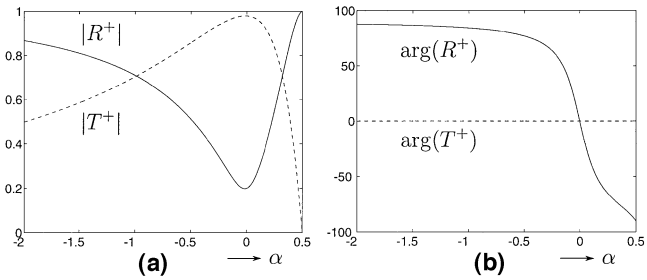

FIG. 3. Modulus (a) and phase (b) as a function of α of the reflection and transmission coefficients (flux normalized) of a two-sided singularity, with c_n, ϱ_n, z_n given in Table 1.

for pressure as well as power flux normalization. Bear in mind that only positive frequencies were considered, otherwise equation (31) would have read $R^{\pm} = j\,\mathrm{sign}(\omega)\cos(\nu\pi)$. This implies that for this situation the reflected signal in the time domain is proportional to the Hilbert transform of the incident signal. Note the analogy with the reflection coefficient for a thin homogeneous layer (velocity c, thickness d), embedded between two homogeneous half-spaces, which reads $R^{\pm} \approx 2j\omega R_0 d/c$ (Widess, 1973; de Voogd and den Rooijen, 1983). The latter equation implies that in the time domain the reflected signal is approximately proportional to the time derivative of the incident signal. The main difference between both results is that the thin layer response is frequency dependent, whereas the response of the self-similar singularity is frequency independent.

Next the behavior of the wave field in the space-frequency and the space-time domains is further analyzed. Consider a two-sided singularity described by equation (17), with $\alpha_1 = \alpha_2 = \alpha = -0.4$ and the other parameters defined in Table 1 (see Figure 4). Equations (19), (27), and (28) thus yield $\mu_1 = \mu_2 = \mu = 0.9837$, $R^+ = 0.4528 \times \exp(0.4076\,j\pi)$ and $T^+ = 1.0305$ (pressure normalization). Substituting these values in equation (18) gives $P(z, \omega)$ for all z and ω. The real and imaginary parts of this function are shown in Figures 5 and 6, respectively (the frequency f is defined as $f = \omega/2\pi$). Note the regular behaviour of $P(z, \omega)$ at the singular point $z = 0$. Moreover, note that the different frequency components exhibit the same depth-dependent pattern at different scales. This is a manifestation of the similarity property $P(\beta z, \omega) = P(z, \beta^{1-\alpha}\omega)$ for $\beta > 0$.

Band-limited time-domain solutions are obtained by multiplying the results in Figures 5 and 6 by the spectrum of a Ricker wavelet (with central frequency $f_0 = \omega_0/2\pi = 50$ Hz) and by applying an inverse Fourier transform (actually a much denser frequency sampling was used than shown in Figures 5 and 6). The result is shown in a VSP-like representation in Figure 7. Note that the singular point has been shifted to a depth of $z = 200$ m, and the incident wave at $z = 0$ has been shifted to $t = 0$. This figure clearly shows the downgoing incident and the upgoing reflected wave field above and the downgoing transmitted field below the singular point. The solid lines in Figures 8a and 8b show the reflection response at $z = 0$ m and the transmission response at $z = 400$ m in more detail. Note the significant phase-shift ($0.4076 \times 180 = 73.37^{\circ}$) in the reflection response. Figures 8a and 8b also show the results of numerical modeling using the "reflectivity method" (see, for example, Kennett and Kerry, 1979). For this purpose, the configuration has been approximated by a horizontally layered medium with homogeneous layers, with a layer thickness of $\Delta z = 2$ m; the singular point has been chosen at exactly the half-way point in a layer. The match between the exact response (solid) and the numerically modeled response (+) is quite good, but not perfect. Figures 9a and 9b show a similar comparison after

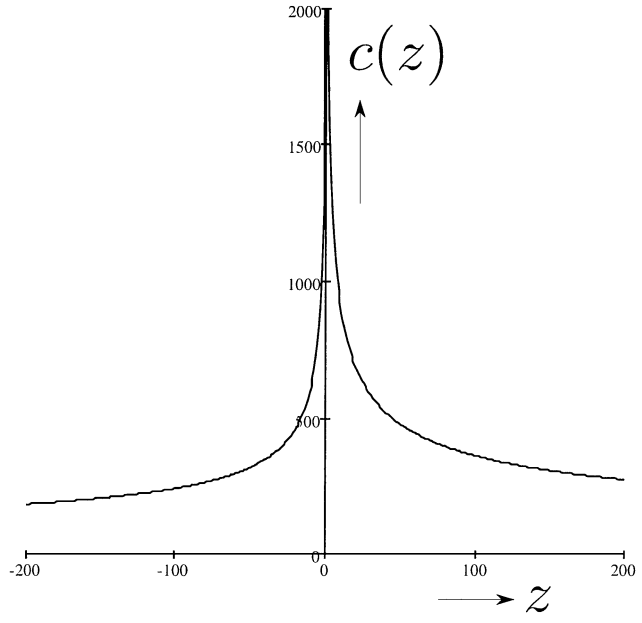

FIG. 4. Two-sided singularity, with $\alpha_1 = \alpha_2 = \alpha = -0.4$, and c_n, ϱ_n, z_n given in Table 1.

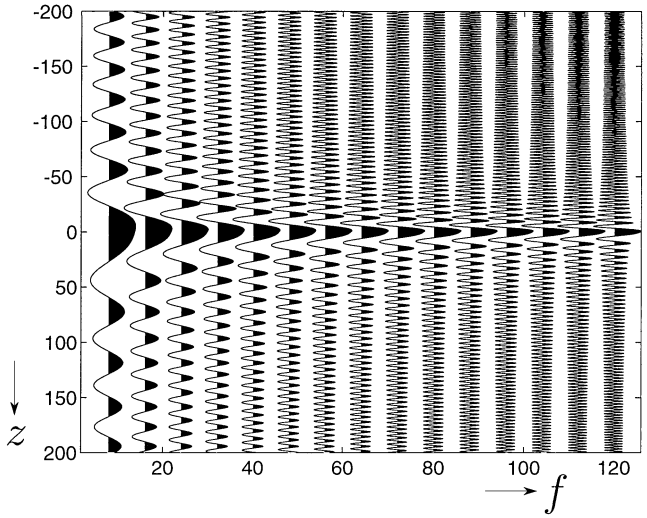

FIG. 5. $\Re\{P(z, 2\pi f)\}$ for the two-sided singularity of Figure 4.

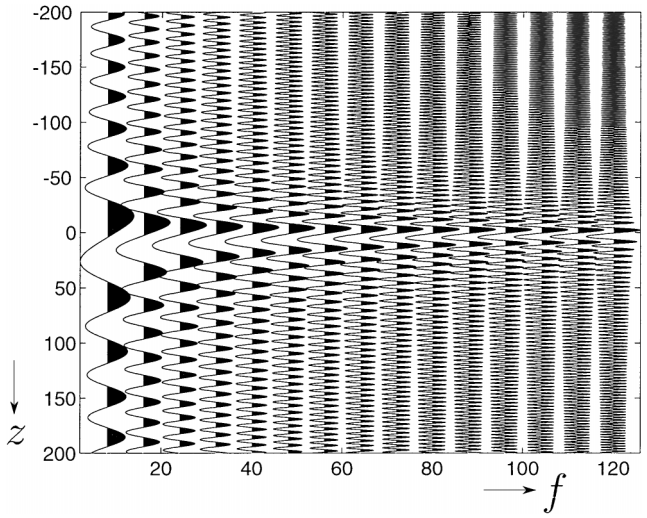

FIG. 6. $\Im\{P(z, 2\pi f)\}$ for the two-sided singularity of Figure 4.

reducing the layer thickness to $\Delta z = 0.2$ m. Note that this time the numerical and analytical results fully overlap.

One-sided singularity

Consider a one-sided singularity with $\alpha_1 = 0$ and $\alpha_2 \neq 0$. Equations (24) and (25) thus yield

$$R^+ = \frac{\frac{\Gamma(\nu)}{\Gamma(1-\nu)}(j\omega\nu|z_2|)^{1-2\nu}\varrho_2 c_2^{2\nu} - \varrho_1 c_1}{\frac{\Gamma(\nu)}{\Gamma(1-\nu)}(j\omega\nu|z_2|)^{1-2\nu}\varrho_2 c_2^{2\nu} + \varrho_1 c_1}, \qquad (33)$$

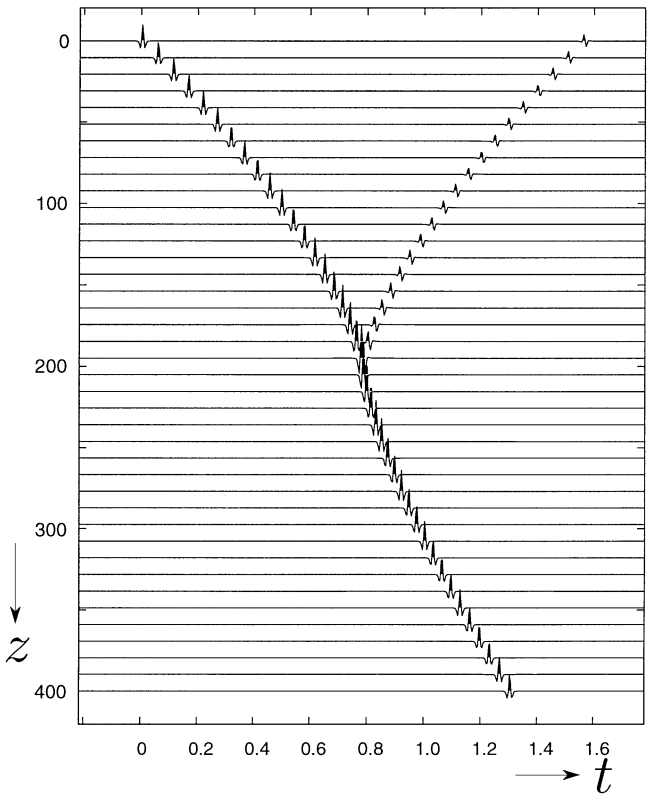

FIG. 7. VSP-like representation of the response of the two-sided singularity of Figure 4. The singular point has been shifted to $z = 200$ m.

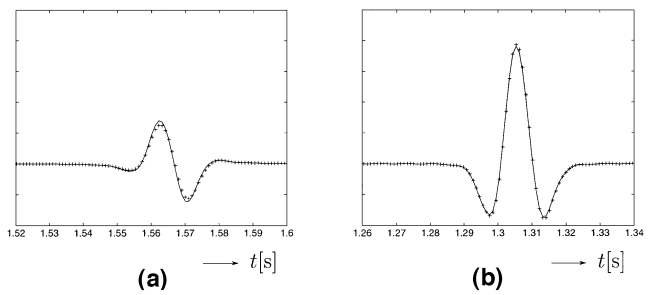

FIG. 8. (a) Analytical (solid) and numerically modeled (+) reflection response at $z = 0$ m. The layer thickness used for the numerical modeling was $\Delta z = 2$ m. (b) Transmission response at $z = 400$ m.

$$T^+ = \begin{cases} \dfrac{\frac{2\Gamma(\nu)}{\Gamma(1-\nu)}(\sqrt{j}\omega\nu|z_2|)^{1-2\nu}\varrho_2 c_2^{2\nu}}{\frac{\Gamma(\nu)}{\Gamma(1-\nu)}(j\omega\nu|z_2|)^{1-2\nu}\varrho_2 c_2^{2\nu} + \varrho_1 c_1} & \text{pressure normalization} \\ \dfrac{\frac{2\sqrt{\pi}}{\Gamma(1-\nu)}\sqrt{(j\omega\nu|z_2|)^{1-2\nu}\varrho_2 c_2^{2\nu}\varrho_1 c_1}}{\frac{\Gamma(\nu)}{\Gamma(1-\nu)}(j\omega\nu|z_2|)^{1-2\nu}\varrho_2 c_2^{2\nu} + \varrho_1 c_1} & \text{power flux normalization,} \end{cases} \qquad (34)$$

with $\nu = \nu_2 = 1/(2 - 2\alpha_2)$. In a similar way, the coefficients R^- and T^- can be obtained. Note that these expressions are frequency dependent, unlike the coefficients in equations (27) and (28) for the two-sided singularity. The factors $(j\omega)^{1-2\nu}$ correspond to a fractional differentiation or integration in the time domain for negative and positive α_2, respectively.

Figure 10 shows a one-sided singularity with $\alpha_2 = -0.4$ and c_n, ϱ_n, z_n defined in Table 1. The frequency-dependent modulus and phase of the coefficients R^+ and T^+ are shown in Figure 11.

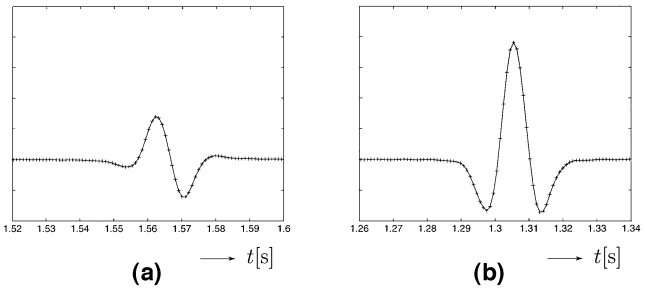

FIG. 9. As in Figure 8, but with $\Delta z = 0.2$ m.

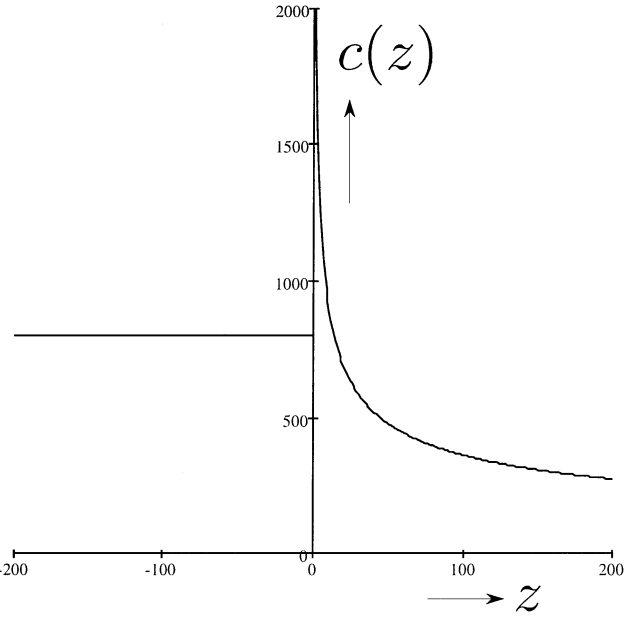

FIG. 10. One-sided singularity with $\alpha_1 = 0, \alpha_2 = -0.4$ and c_n, ϱ_n, z_n given in Table 1.

Figure 12 shows the response of the one-sided singularity in the space-time domain in a VSP-like representation. The singular point has been shifted to a depth of $z = 200$ m and the incident wave at $z = 0$ was again a Ricker wavelet with a central frequency of 50 Hz.

Figures 13a and 13b show the reflection response at $z = 0$ m and the transmission response at $z = 400$ m in more detail, together with the numerically obtained responses (the layer thickness was $\Delta z = 0.2$ m). Note that the numerical and analytical results again fully overlap.

Embedded two-sided singularity

In practice, the parameterization of a singularity, as described by equation (17), will be useful only in a finite region around the singular point. Consider a two-sided self-similar singularity, embedded between two homogeneous half-spaces, where

$$c(z) = \begin{cases} c_1 & \text{for } z \le z_1 \\ c_1|z/z_1|^{\alpha} & \text{for } z_1 < z < 0 \\ c_2|z/z_2|^{\alpha} & \text{for } 0 < z < z_2 \\ c_2 & \text{for } z_2 \le z, \end{cases} \tag{35}$$

with $\alpha < \frac{1}{2}$ (the density is defined again as a step function from ϱ_1 to ϱ_2). For this configuration, the normal incidence reflection and transmission coefficients are derived in a companion paper (Wapenaar, 1998). The resulting expressions are quite involved and are not repeated here. They appear to be frequency dependent. For $\omega \to 0$, the effect of the singularity vanishes; hence, the expressions reduce to the usual coefficients for two homogeneous half-spaces. On the other hand, for $\omega \to \infty$, the effect of the embedding half-spaces vanishes; hence, the expressions reduce to those defined in equations (27)–(30).

For the parameters given in Table 1 and $\alpha = -0.4$, the embedded singularity is shown in Figure 14. The modulus and phase

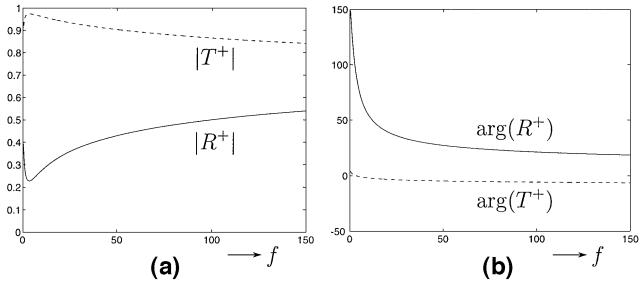

FIG. 11. Modulus (a) and phase (b) as a function of frequency of the reflection and transmission coefficients (flux normalized) of the one-sided singularity of Figure 10.

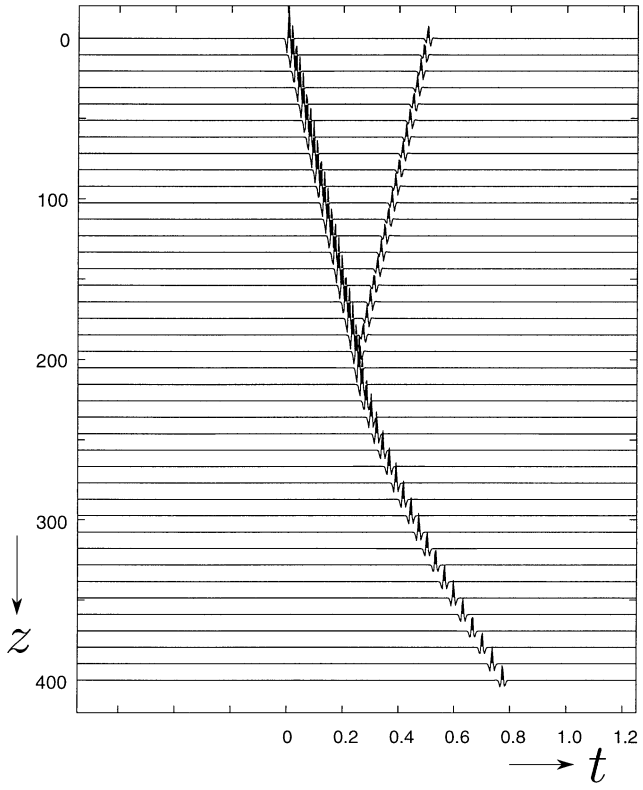

FIG. 12. VSP-like representation of the response of the one-sided singularity of Figure 10. The singular point has been shifted to $z = 200$ m.

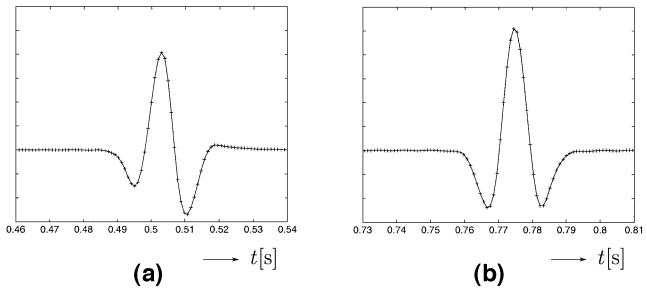

FIG. 13. (a) Analytical (solid) and numerically modeled (+) reflection response at $z = 0$ m. The layer thickness used for the numerical modeling was $\Delta z = 0.2$ m. (b) Transmission response at $z = 400$ m.

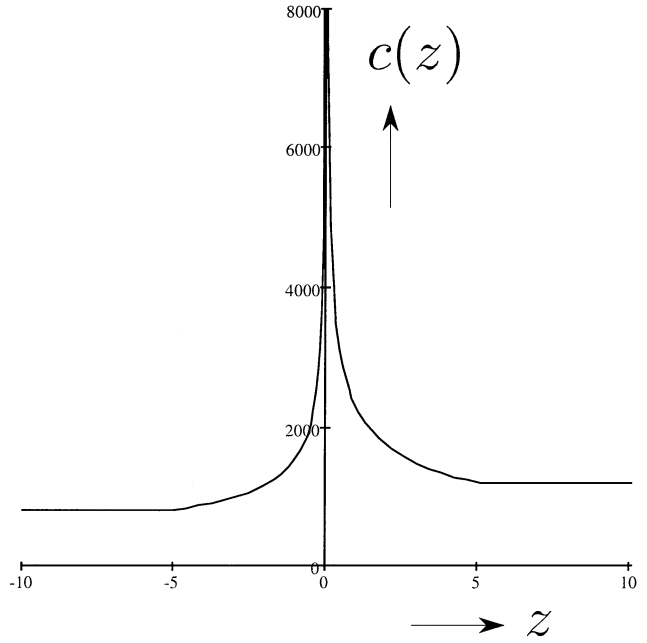

FIG. 14. The self-similar two-sided singularity of Figure 4, embedded between two homogeneous half-spaces.

of the corresponding frequency dependent reflection coefficient are shown in Figures 15a and 15b, respectively. The zero-frequency limit is given by $R^+ \to (c_2 - c_1)/(c_2 + c_1) = 0.2$, which is the reflection coefficient of a step function. The high-frequency approximations, denoted by the dashed lines in Figures 15a and 15b, are $|R^+| \to 0.4528$ and $\arg(R^+) \to 73.37^\circ$. The latter result, which can be written as $R^+ \to 0.4528 \times \exp(0.4076 j\pi)$, corresponds to the reflection coefficient of the singular function of Figure 4, without the embedding half-spaces.

The exact reflection response at $z_1 = -5$ m and the exact transmission response at $z_2 = 5$ m of the embedded singularity of Figure 14 are represented by the solid lines in Figures 16a and 16b (the incident wave was again the Ricker wavelet with a central frequency of 50 Hz). For the same configuration, the high-frequency approximations of these responses have been computed with the coefficients of equations (27) and (28). The results are denoted by the crosses (+) in Figures 16a and 16b. Note that the main features of the exact responses are reasonably well reproduced by these high-frequency approximations. Reversing the argument, one can state that the embedding half-spaces do not significantly change the response described by equations (27) and (28).

OBLIQUE INCIDENCE REFLECTION AND TRANSMISSION COEFFICIENTS

The wave equation for oblique propagation is

$$\left[\frac{\partial^2}{\partial z^2} + \omega^2\left(\frac{1}{c^2(z)} - p^2\right)\right] P(z, p, \omega) = 0, \qquad (36)$$

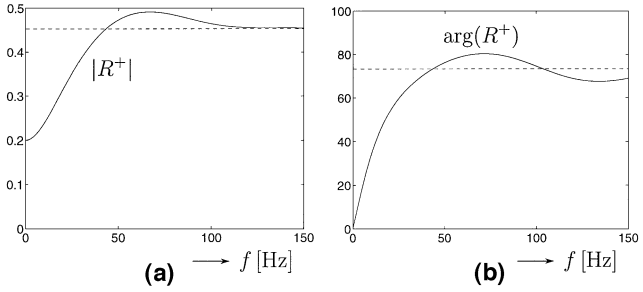

FIG. 15. Modulus (a) and phase (b) as a function of frequency of the reflection and transmission coefficients (flux normalized) of the embedded singularity of Figure 14 (solid) and their high-frequency approximations (dashed).

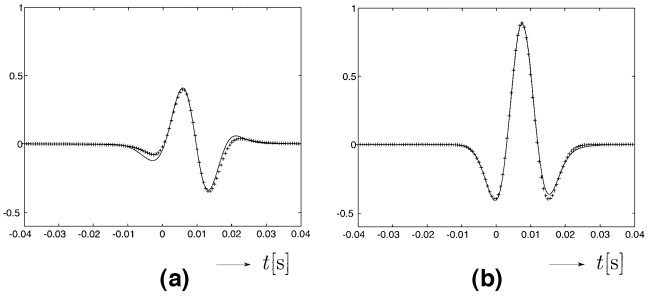

FIG. 16. (a) Exact (solid) and high-frequency approximation (+) of the reflection response of the embedded singularity of Figure 14. (b) Transmission response.

where p denotes the raypath parameter; it is related to the depth-dependent propagation angle $\theta(z)$ via $p = [\sin\theta(z)]/c(z)$. In the following, $c(z)$ represents again the self-similar singularity, described by equation (17), with $\alpha_1 = \alpha_2 = \alpha$.

Analogous to equation (18), reflection and transmission coefficients are formally introduced via

$$P(z, p, \omega) = \begin{cases} \mu_1(p, \omega)\{U_1(z, p, \omega) + R^+(p, \omega)U_1^*(z, p, \omega)\}, & z < 0, \\ \mu_2(p, \omega)T^+(p, \omega)U_2^*(z, p, \omega), & z > 0, \end{cases} \qquad (37)$$

where $U_n(z, p, \omega)$ for $n = 1$ and $n = 2$ denote elementary solutions of equation (36) in the half-spaces $z < 0$ and $z > 0$, respectively. Closed-form expressions for $U_n(z, p, \omega)$ are not available. Therefore, this approach does not lead to unique solutions for R^+ and T^+. However, it will turn out that it leads to unique self-similarity relations for R^+ and T^+.

Replacing z by βz (with $\beta > 0$) in equation (36) yields

$$\left[\frac{1}{\beta^2}\frac{\partial^2}{\partial z^2} + \omega^2\left(\frac{1}{c^2(\beta z)} - p^2\right)\right] P(\beta z, p, \omega) = 0. \qquad (38)$$

Substituting $c(\beta z) = \beta^\alpha c(z)$ and multiplying the result by β^2 gives

$$\left[\frac{\partial^2}{\partial z^2} + (\beta^{1-\alpha}\omega)^2\left(\frac{1}{c^2(z)} - (\beta^\alpha p)^2\right)\right] P(\beta z, p, \omega) = 0. \qquad (39)$$

The term between the square brackets is the same as in equation (36), with ω replaced by $\beta^{1-\alpha}\omega$ and p replaced by $\beta^\alpha p$. Hence, equation (39) is satisfied by $P(z, \beta^\alpha p, \beta^{1-\alpha}\omega)$ as well as $P(\beta z, p, \omega)$. Of course these solutions are not necessarily equal. However, the elementary solutions $U_n(z, p, \omega)$ that constitute $P(z, p, \omega)$ [see equation (37)] can be chosen such that they obey the similarity relation

$$U_n(\beta z, p, \omega) = U_n(z, \beta^\alpha p, \beta^{1-\alpha}\omega). \qquad (40)$$

Note that this result applies to propagating as well as evanescent waves.

For the derivation of the similarity relations for the reflection and transmission coefficients, some more relations are needed. From equation (40), it follows that

$$U_n'(\beta z, p, \omega) = \beta^{-1} U_n'(z, \beta^\alpha p, \beta^{1-\alpha}\omega), \qquad (41)$$

where $U_n'(z, p, \omega)$ denotes again the derivative of $U_n(z, p, \omega)$ with respect to z [hence, $U_n'(\beta z, p, \omega)$ denotes the derivative with respect to βz]. Using equations (40) and (41), it follows that the power flux $F_n(z, p, \omega)$, defined analogous to equation (10), obeys

$$F_n(\beta z, p, \omega) = \beta^{-\alpha} F_n(z, \beta^\alpha p, \beta^{1-\alpha}\omega). \qquad (42)$$

For the normalization coefficient $\mu_n(p,\omega)$, defined analogous to equation (19), the following similarity relation is obtained:

$$\mu_n(p,\omega) = \begin{cases} \mu_n(\beta^\alpha p, \beta^{1-\alpha}\omega) & \text{pressure normalization} \\ \beta^{\alpha/2}\mu_n(\beta^\alpha p, \beta^{1-\alpha}\omega) & \text{power flux normalization.} \end{cases} \tag{43}$$

Finally, replacing ϵ by $\beta\epsilon$ in the p-dependent equivalent of boundary conditions (20) and (21), substituting similarity relations (40)–(43), and comparing the result with the original boundary conditions, the following relations are obtained:

$$R^+(p,\omega) = R^+(\beta^\alpha p, \beta^{1-\alpha}\omega), \tag{44}$$

$$T^+(p,\omega) = T^+(\beta^\alpha p, \beta^{1-\alpha}\omega). \tag{45}$$

Similar results can be derived for R^- and T^-. For $\alpha = 0$ (i.e., for homogeneous half-spaces), equations (44) and (45) imply that the reflection and transmission coefficients are frequency independent (as expected). For arbitrary α, equations (44) and (45) state that the reflection and transmission coefficients are constant along curves described by (see Figure 17)

$$p^{1-\alpha}\omega^{-\alpha} = \text{constant}. \tag{46}$$

Note that these curves are fully determined by the singularity exponent α.

Angle-dependent responses

For the two-sided singularity of Figure 4, the angle-dependent reflection and transmission responses have been modeled with the reflectivity method. The wavelet of the incident field was again a Ricker wavelet with a central frequency of 50 Hz. The results in the p,τ-domain are shown in Figures 18a and 18b, respectively. The traces at $p = 0$ correspond to those in Figures 9a and 9b. The angle-dependent reflection coefficient $R^+(p,\omega)$ is retrieved from the Fourier transform of the reflection response in Figure 18a, divided by the spectrum of the Ricker wavelet. The modulus $|R^+(p,\omega)|$ is shown in Figure 19a. Contours of constant $|R^+(p,\omega)|$ are shown in Figure 19b. These contours follow the analytical curves in Figure 17 (for $\alpha = -0.4$) very accurately.

A similar numerical experiment has been done for the embedded singularity shown in Figure 14. The reflection and transmission responses are shown in Figures 20a and 20b, respectively. The traces at $p = 0$ correspond to those in Figures 16a and 16b. The modulus of the angle-dependent reflection coefficient and its contours are shown in Figures 21a and 21b, respectively. In Figure 21a, the behavior for $p = 0$ corresponds to the analytical result of Figure 15a. For $\omega \to 0$, the p-dependent behavior corresponds to the Zoeppritz result for two homogeneous half-spaces, i.e., the effect of the singularity vanishes. On the other hand, for large ω the results match those of the previous example, which implies that the effect of the embedding half-spaces vanishes.

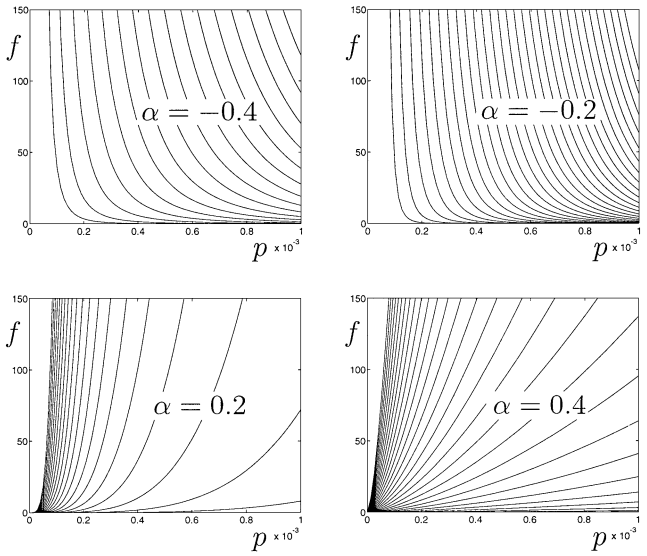

FIG. 17. Curves along which the reflection and transmission coefficients $R^\pm(p, 2\pi f)$ and $T^\pm(p, 2\pi f)$ are constant.

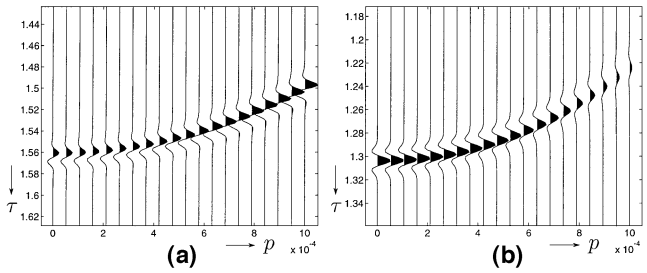

FIG. 18. (a) Angle-dependent reflection response of the singular function of Figure 4. (b) Transmission response.

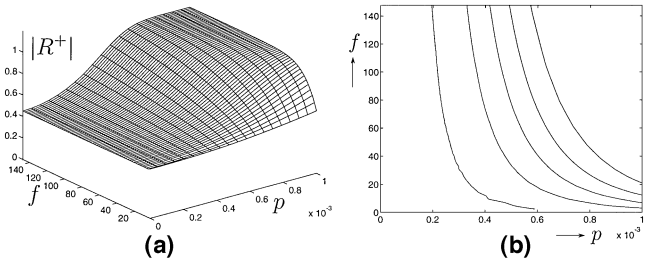

FIG. 19. (a) $|R^+(p, 2\pi f)|$, obtained from the Fourier transform of Figure 18a. (b) Contours of constant $|R^+(p, 2\pi f)|$, obtained from (a). Compare with Figure 17 for $\alpha = -0.4$.

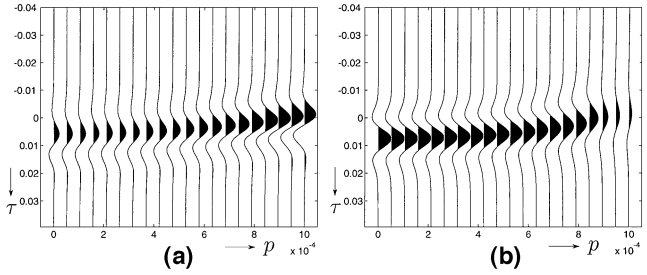

FIG. 20. (a) Angle-dependent reflection response of the embedded singularity of Figure 14. (b) Transmission response.

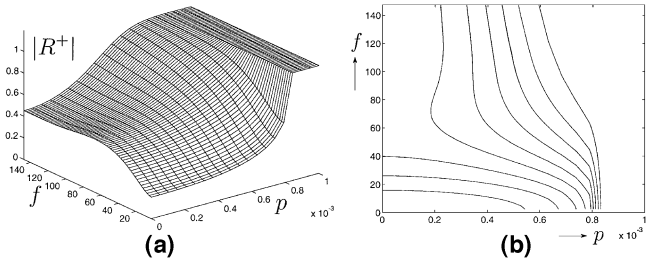

FIG. 21. (a) $|R^+(p, 2\pi f)|$, obtained from the Fourier transform of Figure 20a. (b) Contours of constant $|R^+(p, 2\pi f)|$, obtained from (a).

DISCUSSION

In this paper, outliers in well logs have been parameterized by self-similar singularities, since the wavelet transform of this type of singularity (Mallat and Hwang, 1992) reveals similar properties as that of several outliers in well logs (Herrmann, 1997). Of course, this parameterization represents nothing more than a simplified model for "true" interfaces. In particular, this model will be valid at most in a finite depth interval; moreover, in reality the velocity will not go to infinity. Hence, the parameterization will only be valid for a limited range of scales (in the wavelet transform domain). As a consequence, in practice the expressions for the reflection and transmission coefficients are applicable only for a finite range of frequencies (scale σ is proportional to the inverse frequency: $\sigma \propto 1/\omega$). Of course, the main question is whether or not the derived results are applicable in the seismic frequency range. To some extent this point has been addressed in the examples of the embedded singularity. It turned out that the embedding half-spaces (a large scale effect) do not seriously affect the seismic reflection and transmission responses (Figure 16). In a companion paper (Wapenaar, 1998), the relation between the scale properties of the singularity and the bandwidth of the reflected and transmitted wave field is further analyzed. Among others things, that paper shows that smoothing of the singularity (a small-scale effect) has hardly any effect on the response, provided that the smoothing does not affect the scales corresponding to the seismic frequency range.

Another intriguing question is to what extent the expressions for the angle-dependent behavior [equations (44)–(46)] are applicable to the response of actual well-log singularities. Since these singularities never occur in isolation, their response should preferably be analyzed in the wavelet transform domain rather than in the frequency domain. Using the property $\sigma \propto 1/\omega$, it follows from equation (46) that in the wavelet transform domain the reflection and transmission coefficients are constant along curves described by

$$p^{1-\alpha}\sigma^{\alpha} = \text{constant}. \tag{47}$$

In a recent paper (Wapenaar et al., 1997), we modeled the angle-dependent response of a real well log (Figure 1) in the seismic frequency range (5–100 Hz), applied a transformation to the p, z-domain (angle-dependent migration), and analyzed the result with the wavelet transform (analogous to Dessing et al., 1996). At selected depth levels (corresponding to outliers in the well log), the contours in the p, σ-plane showed a behavior that is approximately described by equation (47). The singularity exponents α, derived from these contours, correspond within 20% to those derived directly from the well log. The further development of this characterization method is subject of current research (Goudswaard and Wapenaar, 1998).

CONCLUSIONS

The reflection and transmission coefficients of self-similar interfaces have been analyzed. For normal incidence, analytical expressions have been obtained, which reduce to the usual expressions when the singularity exponents α_1 and α_2 are equal to zero. For two-sided singularities with $\alpha_1 = \alpha_2$, the expressions become frequency independent. For this situation, the phase of the reflection coefficient is largely determined by the factor j [see equation (27)], which corresponds to a Hilbert transform in the time domain. For one-sided singularities ($\alpha_1 = 0, \alpha_2 \neq 0$), the expressions for the reflection and transmission coefficients contain the frequency-dependent factor $(j\omega)^{1-2\nu}$, which corresponds to a fractional differentiation or integration in the time domain for negative and positive α_2, respectively. For two-sided singularities embedded between homogeneous half-spaces, the reflection and transmission coefficients are also frequency dependent. In the high-frequency limit, they behave as discussed above; in the low-frequency limit, they reduce to the coefficients of a step-function interface.

For oblique incidence, no closed-form expressions have been found. Exploiting the self-similarity property of the interface, it has been shown that the reflection and transmission coefficients are constant along curves described by $p^{1-\alpha}\omega^{-\alpha} = \text{constant}$ (or in the wavelet transform domain, along curves described by $p^{1-\alpha}\sigma^{\alpha} = \text{constant}$). The singularity exponent α that is reflected in these curves may prove to be a useful indicator in seismic characterization.

ACKNOWLEDGMENTS

I thank the Dutch Technology Foundation (STW) for their financial support and Professor Jacob Fokkema for many fruitful discussions.

REFERENCES

Abramowitz, M., and Stegun, I. A., 1970, Handbook of mathematical functions: Dover Publ., Inc.
Aki, K., and Richards, P. G., 1980, Quantitative seismology, **I**: W. H. Freeman & Co.
Brekhovskikh, L. M., and Godin, O. A., 1990, Acoustics of layered media. Part 1. Plane and quasi-plane waves: Springer.
Castagna, J. P., and Backus, M. M., 1993, Offset-dependent reflectivity—Theory and practice of AVO analysis: Soc. of Expl. Geophys.
De Voogd, N., and den Rooijen, H., 1983, Thin layer response and spectral bandwidth: Geophysics, **48**, 12–18.
Dessing, F. J., Hoekstra, E. V., Herrmann, F. J., and Wapenaar, C. P. A., 1996, Multiscale edge detection by means of multiscale migration: 66th Ann. Internat. Mtg., Soc. Expl. Geophys., Expanded Abstracts, 459–462.
Goudswaard, J. C. M., and Wapenaar, C. P. A., 1998, Characterization of reflectors by multi-scale amplitude and phase analysis of seismic data: 68th Ann. Internat. Mtg., Soc. Expl. Geophys., Expanded Abstracts, 1688–1691.
Hargreaves, N., 1996, Some geophysical consequences of fractal scaling: 58th Mtg., Eur. Assoc. Geosc. & Engineers, Extended Abstracts, Session X025.
Herrmann, F. J., 1997, A scaling medium representation: Ph.D. thesis, Delft Univ. of Technology.

Kennett, B. L. N., and Kerry, N. J., 1979, Seismic waves in a stratified half-space: Geoph. J. Roy. Astr. Soc., **57**, 557–584.
Mallat, S. G., and Hwang, W. L., 1992, Singularity detection and processing with wavelets: IEEE Trans. Inform. Theory, **38**, 617–643.
Wapenaar, C. P. A., 1998, Seismic reflection and transmission coefficients of a self-similar interface: Geophys. J. Internat., **135**, 585–594.
Wapenaar, C. P. A., van Geloven, W. J. F., Goudswaard, J. C. M., van Wijngaarden, A. J., and Dessing, F. J., 1997, AVA migration and multiscale characterization in finely layered media: J. Seis. Expl., **6**, 181–198.
Widess, M. B., 1973, How thin is a thin bed?: Geophysics, **38**, 1176–1180.
Zoeppritz, K., 1919, Erdbebenwellen VIIIB, On the reflection and propagation of seismic waves: Göttinger Nachrichten, **1**, 66–84.

APPENDIX A

LIMITS OF THE ELEMENTARY SOLUTION

Using equations (6), (9), and (13), as well as equations (9.1.3) and (9.1.10) of Abramowitz and Stegun (1970), the following series expansions for the elementary solution and its derivative are obtained:

$$U(z,\omega) = \sum_{m=0}^{\infty} a_m \zeta^{2m} + \sum_{m=0}^{\infty} b_m \zeta^{2(m+\nu)}, \tag{A-1}$$

and

$$\frac{\partial U(z,\omega)}{\partial z} = \frac{\omega}{c_1}\chi^{2\nu-1}\mathrm{sign}(z) \times \left[\sum_{m=1}^{\infty} 2m a_m \zeta^{2(m-\nu)} + \sum_{m=0}^{\infty} 2(m+\nu) b_m \zeta^{2m}\right], \tag{A-2}$$

where

$$a_m = \frac{\mathrm{e}^{j\left(\nu-\frac{1}{2}\right)\frac{\pi}{2}}(-1)^m 2^{-(2m-\nu)}}{\sin(\nu\pi)m!\Gamma(m+1-\nu)}, \tag{A-3}$$

$$b_m = \frac{-\mathrm{e}^{-j\left(\nu+\frac{1}{2}\right)\frac{\pi}{2}}(-1)^m 2^{-(2m+\nu)}}{\sin(\nu\pi)m!\Gamma(m+1+\nu)}. \tag{A-4}$$

The limits for $|z| \to 0$ exist when all exponents of ζ in equations (A-1) and (A-2) are nonnegative and the denominators in equations (A-3) and (A-4) are nonzero. These conditions are fulfilled when $0 < \nu < 1$, i.e., when $\alpha < \frac{1}{2}$. Hence, the limits for $|z| \to 0$ are expressed in terms of a_0 and b_0 according to

$$U(z,\omega) \to A, \tag{A-5}$$

$$\frac{\partial U(z,\omega)}{\partial z} \to \frac{2\omega\nu}{c_1}\chi^{2\nu-1}\mathrm{sign}(z)B, \tag{A-6}$$

where, using equations (6.1.15) and (6.1.17) of Abramowitz and Stegun (1970),

$$A \equiv a_0 = \frac{\mathrm{e}^{j\left(\nu-\frac{1}{2}\right)\frac{\pi}{2}}2^{\nu}}{\sin(\nu\pi)\Gamma(1-\nu)} = \frac{\mathrm{e}^{j\left(\nu-\frac{1}{2}\right)\frac{\pi}{2}}2^{\nu}\Gamma(\nu)}{\pi}, \tag{A-7}$$

$$B \equiv b_0 = \frac{-\mathrm{e}^{-j\left(\nu+\frac{1}{2}\right)\frac{\pi}{2}}2^{-\nu}}{\sin(\nu\pi)\Gamma(1+\nu)} = \frac{-\mathrm{e}^{-j\left(\nu+\frac{1}{2}\right)\frac{\pi}{2}}\Gamma(1-\nu)}{2^{\nu}\nu\pi}. \tag{A-8}$$